ELSEVIER

Advances in Colloid and Interface Science 134–135 (2007) 125 – 137

ADVANCES IN COLLOID AND INTERFACE SCIENCE

www.elsevier.com/locate/cis

Bubble dynamics during the non-isothermal degassing of liquids. Exploiting microgravity conditions

Margaritis Kostoglou, Thodoris D. Karapantsios *

Division of Chemical Technology, Department of Chemistry, Aristotle University of Thessaloniki, University Box 116, 541 24 Thessaloniki, Greece

Available online 8 May 2007

Abstract

This work reviews the up to date state of understanding of dynamic phenomena occurring when gas bubbles grow over submerged heated surfaces. Gas bubbles are produced on hot surfaces because the adjacent liquid layers become superheated causing local desorption of dissolved gases while the liquid far afield remains at low temperatures. Non-isothermal degassing is a very complex process combining heat and mass transport coupled with momentum exchange between the two phases. Difficulties due to buoyancy effects on gas bubbles as well as natural convection of hot liquid layers hindered its thorough investigation in terrestrial conditions and only recent microgravity data allowed serious progress to be made. To reduce the complexity, gas bubble growth on a heated wall was studied here separately from bubble lateral motion and coalescence. A complete mathematical formulation was provided but given the inability to solve the problem numerically with the present resources, a series of approximate solutions were attempted. The comparison between experimental observations and theoretical predictions revealed useful information regarding the governing mechanisms of bubble growth.

Keywords: Bubble growth; Diffusion; Heat transfer; Mass transfer; Low gravity; Carbonated liquids

Contents

1. Introduction

Understanding the dynamics of bubble growth during desorption of dissolved gases (degassing) in liquids is significant for the effective design of many industrial applications. In many applications degassing is caused by a reduction of system pressure at ambient temperature, e.g. in cavitating turbines and pumps [1], in carbonated drinks [2], and in liquid waste treatment by dissolved air flotation [3]. In another class of applications desorption of dissolved gases is caused by raising the system temperature, e.g. in the degassing of glass melts and glass

* Corresponding author.
E-mail address: karapant@chem.auth.gr (T.D. Karapantsios).

0001-8686/$ - see front matter © 2007 Elsevier B.V. All rights reserved.
doi:10.1016/j.cis.2007.04.027

powders [4,5], in the degassing of alloy powders [6], and in the degassing of metal–carbon selective surfaces [7]. Moreover, in many thermal processes, e.g. heat exchangers, boilers, distillation columns, spray dryers etc., thermal degassing of liquid layers is a detrimental side-effect which reduces liquid heat transfer coefficients and evaporation rates by forming layers of air over hot surfaces [8,9]. While decompression degassing has a global volume effect, thermal degassing is usually imposed locally through hot vessel walls or submerged heaters and so inevitably yields temperature gradients (non-isothermal conditions) across the liquid volume. Using partial vacuum to enhance degassing lowers but does not extinct temperature gradients [10,11].

Early studies on bubble growth dynamics were performed having in mind vapor bubbles controlled by heat transfer (nucleate boiling) rather than dissolved gas bubbles where mass transfer dominates (desorption). Despite the significant differences between nucleate boiling and desorption in the involved time scales and the underlying physical mechanisms, there are also a few points in common: the momentum exchange between an expanding bubble and the surrounding liquid and a qualitative analogy between heat and mass transfer. Several of those pioneering studies focused on the spherically symmetric growth of single, isolated, bubbles controlled by heat transfer inside infinite liquids of constant superheat [12,13]. Among the few reported analytical solutions, the simple parabolic law ($R \sim t^{n=0.5}$, where R is the bubble radius and t the time of growth) introduced by Scriven [14] has been particularly successful in describing single bubble growth in uniform temperature fields, i.e., during nucleate boiling. The same expression proved also useful in describing the quasi-isothermal mass-diffusion induced bubble growth from supersaturated (with dissolved gas) solutions during their global decompression [2,15–18].

Yet, there is experimental evidence in the boiling literature that the exponent n can vary over a broad range of values e.g. from $\sim 0.3 < n < \sim 0.75$ [19,20], a fact which was partially attributed to experimental difficulties because of the very short time scales involved in boiling bubble production. Even the boiling experiments of [21] in a microgravity environment, where temperature (density) driven convection was diminished, gave a value of n close to 0.4 but of course the vigorous agitation created by fast expanding bubbles was once more present. The diversity in the reported values of n for nucleation boiling reflects both difficulties in performing well-controlled experiments in such short time scales and also possible contributions from several rate-controlling mechanisms such as surface tension, viscosity and inertia.

Slowly growing single bubbles due to desorption of dissolved gases in supersaturated solutions follow quite accurately the parabolic growth law [17,18]. However, deviations from it were witnessed even in quasi-uniform temperature fields when multiple bubbles (met in most industrial processes) are produced [22,23]. Exponents down to $n \sim 0.3$ and irregular growth curves were observed and were attributed to bubble coalescence between neighboring nucleation sites.

Unfortunately, on earth the study of bubble growth is complicated by various factors. Even under isothermal conditions (bubble production triggered by decompression) buoyancy soon drives the bubble away from its nucleation site in a direction opposite to gravity. So, only small bubbles and for a brief period of time after their formation can be monitored before departure from their nucleation site. From a practical point of view this means that one should use fast cameras and high magnifications at the cost of reduced spatial resolution. From a physical point of view this means that one can monitor only high and unstable growth rates as a result of the transient initial growth after nucleation. In addition, decompression has a global effect in the sample volume which may lead to an uncontrollable production of many simultaneous bubbles that can obscure observation and complicate the concentration field around the bubbles. Distortion of bubble shape from sphericity under the influence of gravity is usually a less dramatic effect (due to the possibility of small bubbles) but yet unavoidable. Using a small submerged heater to create local supersaturation and so have a bubble standing at a specific location (nucleation site) of the heater alleviates the situation but then the presence of gravity can impose significant natural convection currents around the heater. To surmount all these problems it is necessary to conduct experiments in weightlessness. This unique environment (1) allows to suppress natural convection of liquid thermal layers, (2) let bubbles grow up to large sizes without departing from the heater (field of view) and (3) avoids bubble shape distortion.

In a series of ESA (European Space Agency) Parabolic Flight Campaigns, Karapantsios and co-workers [24–26] exploited the low-g conditions achieved during the free-fall of an airplane to study the slower (compared to boiling) bubble dynamics during degassing of several liquids. Bubble production was triggered by heat pulses given to a miniature submerged heater which raised the liquid temperature locally creating supersaturation of dissolved gas over the surface of the heater. Far-off, the bulk liquid remained unaffected (at saturation conditions). Under such non-isothermal but well controlled conditions, it was found that the growth rate of single bubbles deviates from the parabolic law to an extent depending on the liquid's physical and transport properties; the slowest the growth rate the nearest to $n = 0.5$. Thus, the interplay between heat and mass transfer during the expansion of a bubble into the surrounding liquid can cause a departure from the ideal parabolic law. Further deviations from the parabolic law were observed due to the lateral motion and interaction of bubbles over the surface of the heater. Different behaviors were noticed for spherical and flat plate heaters, the latter being technically and theoretically more difficult to tackle.

The scope of the present work is to present, formulate and analyze the problem of the dynamics of bubble growth during the non-isothermal desorption of a gas from supersaturated solutions. Data from the low-g experiments of Karapantsios and co-workers will be employed to demonstrate the features of the problem. To our knowledge, these were the first experiments of diffusion-induced bubble production of a dissolved gas that were performed in weightlessness. Further to that, some of these experiments were conducted at temperatures a little below the boiling temperature of the liquids where also the contribution of vapor pressure was significant. Such information is important for the interpretation of bubble dynamics during subcooled boiling at high superheats.

The outline of the work is as follows: First, the general problem is described qualitatively based on the experimental

observations and it is decomposed in constituent sub-problems. Each one of these is analyzed according to the current stage of knowledge in the literature and in particular the growth sub-problem is formulated in detail by deriving the appropriate set of equations since it is a rather unusual one. Then the experimental set up is presented shortly. Finally, several approximate solutions to the growth problem are presented in a hierarchical manner and their results are discussed in relation to experimental data.

2. Theory

2.1. General

Several phenomena occur over a heated surface that is immersed in a liquid saturated with a dissolved gas in a microgravity environment. These phenomena take place simultaneously or sequentially depending on the particular set of conditions (heat flux, gas–liquid system). In the case of a free-of-gas liquid, turning on the power supply would simply rise the temperature of the heater up to the point of thermal equilibrium between the input heat and the heat losses to the liquid (through conduction in the absence of gravity). But for the case of a gas saturated liquid, at some moment during the elevation of the heater's temperature, bubble nucleation takes place. This nucleation can be of quasi-homogeneous or of heterogeneous nature [27,28]. The main difference between the two types of nucleation is that in the former the nucleation occurs at random positions on the surface of the heater whereas in the latter the bubbles are generated always at the same preferential positions requiring lower energy. These preferential positions are usually surface defects which retain gas pockets from previous nucleation events. Once a bubble appears on the surface of the heater, it grows in a very specific way determined by heat and mass transfer and by the local geometry. There are cases that the growing bubble at some moment depins from its nucleation site and starts to move across the hot solid surface. In cases of single bubble generation (e.g., at low heat fluxes) the bubble leaves the surface (due to g-jitters) before the generation of the next bubble. In cases of multiple bubbles generation (e.g., at high heat fluxes), a coalescence step usually precedes the detachment. Obviously, the above phenomena cannot be analyzed simultaneously so it is important to examine them one at a time in order to understand the cause and the corresponding driving mechanism for each one of them. The sequence of the occurring phenomena is shown schematically in Fig. 1. The double arrow denotes the phenomena that may occur simultaneously for the same bubble. The emphasis here is to the phenomena described in the shaded boxes.

2.2. Bubble growth

2.2.1. Simplifications

The mechanism of the non-isothermal bubble growth is complicated and certainly different from the isothermal one encountered during decompression, combining heat and mass transfer, phase change and fluid dynamics. Based on experimental observations of Karapantsios and co-workers [24–26] and on literature data of contact angle on glass, a slowly growing bubble can be assumed to be of a spherical shape having a point contact (zero contact angle) with the heater (a glass-coated thermistor, see Section 3). The complete physical problem includes:

a) Transient heat conduction equation with a non-linear heat source (temperature-dependent ohmic resistance) in the heater.
b) Navier–Stokes equation in the fluid (liquid and bubble) domains. The liquid motion is set by (i) bubble growth (ii) thermocapillary motion due to a temperature gradient along the bubble surface.
c) Transient convection–diffusion equation for heat and mass transfer in the two fluid domains.

Several simplifications can be made on the physics of the problem based on the values of the ratios of the rates of occurring phenomena and on the values of the ratios of some physicochemical parameters:

1) The heater is assumed to have a uniform (but varying with time t) temperature $T_e(t)$ due to the large ratio of its material thermal diffusivity with respect to the liquid thermal diffusivity.
2) Thermal and mass diffusivity are two orders of magnitude larger in the gas of the bubble than in the surrounding liquid, so transient and convection effects can be ignored inside the bubble compared to the liquid phase.
3) The density and thermal conductivity of the bubble gas are negligibly small in comparison with those of the liquid.
4) The evaporation of liquid on the gas–liquid interface occurs infinitely fast. This means that thermodynamic equilibrium is assumed at the interface, with the assumption of an ideal mixture, so that the mole fraction of the vapor at the interface can be directly related to the instantaneous temperature, and the solute gas concentration in the liquid at every point on the interface is the equilibrium solubility corresponding to the

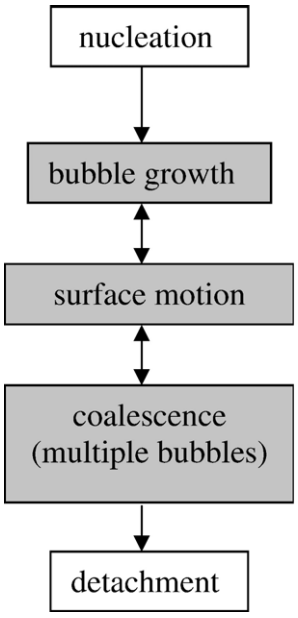

Fig. 1. A schematic of the main phenomena occurring during the degassing on a heated solid surface.

temperature at that point. This leads to variation of the gas phase mole fraction along the interface. In addition, the latent heat of the evaporating liquid can be shown to be insignificant with respect to the heat flux from the heater so it can be ignored.

5) The bubble growth is very slow with respect to flow dynamics so a pseudo steady-state flow field can be assumed.

The geometry of the problem and the definition of the spherical coordinate system used below are shown in Fig. 2. Given the aforementioned assumptions the problem is described in mathematical terms as follows:

2.2.2. Field equations

2.2.2.1. Bubble domain

$$\nabla^2 T_g = 0 \tag{1}$$

$$\nabla^2 x_v = 0 \tag{2}$$

where T_g is the gas temperature and x_v is the vapor molar fraction in the bubble.

2.2.2.2. Liquid domain

$$\text{heat conservation } \rho_\ell c_p \frac{\partial T}{\partial t} + \rho_\ell c_p \vec{u}\vec{\nabla} T = \vec{\nabla} k \vec{\nabla} T \tag{3}$$

$$\text{gas mass conservation (transient) } \frac{\partial c}{\partial t} + \vec{u}\vec{\nabla} c = \vec{\nabla} D \vec{\nabla} c \tag{4}$$

$$\text{continuity equation } \vec{\nabla}\vec{u} = 0 \tag{5}$$

$$\text{Navier} - \text{Stokes (pseudo} - \text{steady state) } \vec{u}\vec{\nabla}\vec{u} = \vec{\nabla} v \vec{\nabla}\vec{u} \tag{6}$$

where T is the liquid temperature, c is the dissolved gas concentration in the liquid and $\vec{u}$ is the velocity field in the liquid. The symbols k,v, and D denote the liquid thermal conductivity, liquid kinematic viscosity and gas-in-liquid diffusion coefficient, respectively. The density ρ_ℓ and the specific heat capacity c_p refer to the liquid phase. It is noted that in the general case k, D and v are not constants but are functions of temperature.

2.2.3. Boundary conditions

2.2.3.1. At S_1 (heater's surface)

$$\textit{heater's} \text{ temperature } T = T_e \tag{7a}$$

$$\text{No slip condition for liquid velocity } \vec{u} = 0 \tag{7b}$$

$$\text{No gas penetratrion condition } \frac{\partial c}{\partial \vec{n}} = 0 \tag{7c}$$

where $\vec{n}$ denotes the direction normal to the surface.

2.2.3.2. At S_2 (bubble surface)

2.2.3.2.1. Liquid side

$$c = c_{eq}(T) \tag{8a}$$

where c_{eq} is the solubility of gas in the liquid at temperature T and pressure P_b (bubble pressure) or equivalently, at partial pressure of gas P_g [29].

$$\text{No heat penetration towards the bubble } \frac{\partial T}{\partial \vec{n}} = 0 \tag{8b}$$

This condition emerges from the small value of the gas-to-liquid thermal conductivities ratio.

The momentum balance at the interface of the bubble (equivalent to the Rayleigh–Plesset equation) under the slow growth conditions prevailing in degassing degenerates to the following condition for the pressure P_b inside the bubble

$$P_b = P_\infty + \frac{2\sigma}{R} \tag{9}$$

where P_∞ is the pressure in the liquid and σ is the surface tension of the gas–liquid interface. The bubble pressure is the sum of the gas pressure P_g and vapor pressure P_L. Surface tension σ has an effect only at the very early stages of growth [30], being insignificant in the period of practical importance for which then $P_b = P_\infty$.

The normal velocity u_n of the liquid on the surface of a bubble which grows keeping constant not its center but a particular point of its surface (contact point with the heater), is

$$u_n = \frac{dR}{dt}(1 + \cos\theta) \tag{10}$$

where θ is the angular coordinate of a system of spherical coordinates r, θ (no φ-dependence is considered due to

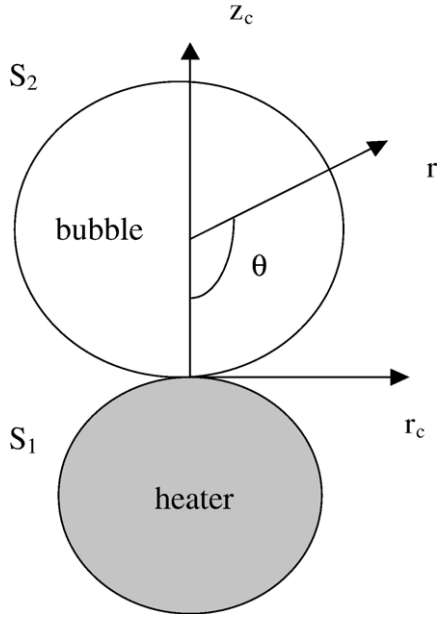

Fig. 2. Schematic and coordinate system definition for the spherical heater–bubble system.

axisymmetry) having as center the center of the bubble. The point $r=R$, $\theta=0$ corresponds to the bubble–heater contact point.

Shear stresses τ_{ns} appear on the surface of the bubble due to the surface distribution of surface tension induced by the surface distribution of temperature. This boundary condition is responsible for the onset of thermo-capillary motion in the liquid.

$$\tau_{ns} = \frac{1}{R}\frac{\mathrm{d}\sigma}{\mathrm{d}\theta} \tag{11}$$

where the index s denotes the local coordinate tangential to the interface.

2.2.3.2.2. Gas side. The local vapor molar fraction at the surface of the bubble can be found from the vapor pressure of the liquid P_L and bubble pressure P_b.

$$x_v = \frac{P_L(T)}{P_b} \tag{12}$$

At the gas/liquid interface, the temperatures of the two fluids must be the same

$$T_g = T \tag{13}$$

2.2.3.3. Far field conditions. For a liquid domain large enough with respect to the size of the heater and the bubble, one can assume an infinite medium with far field temperature and concentration equal to the initial ones (for simplicity, corresponding to saturation conditions).

$$T = T_o \tag{14a}$$

$$c = c_o = c_{eq}(T_o) \tag{14b}$$

2.2.3.4. Total mass balance condition. The global gas balance determines the bubble growth rate as follows:

$$\frac{4\pi}{3}\frac{\mathrm{d}\rho_{gave}R^3}{\mathrm{d}t} = D\int_{S_2}\frac{\partial c}{\partial \vec{n}}\mathrm{d}S \tag{15}$$

where the average gas molar density in the bubble can be found from

$$\rho_{gave} = \frac{1}{V_b}\int_{V_b}(1-x_v)\frac{P_b}{R_g T_g}\mathrm{d}V \tag{16}$$

R_g is the ideal gas constant.

2.2.3.5. Heat balance for the heater. The evolution of the uniform temperature of the heater is given from the following heat balance

$$\rho_s c_{ps} V\frac{\mathrm{d}T_e}{\mathrm{d}t} = Q + hA(T_o - T_e) \tag{17}$$

where Q is the heat per unit of time released at the ohmic resistance of the heater and ρ_s, c_{ps} are the density and specific heat capacity of the material of the heater. V and A are the volume and surface area of the thermistor. Eq. (17) is a very important one determining the final temperature of the heater. In the absence of bubbles, the heat transfer coefficient h corresponds to pure conduction but when a bubble is formed there are also convective contributions due to Marangoni motion initiated by the bubble surface. In this way (as it was inferred theoretically and confirmed experimentally) the bubble initial formation and further development determines the evolution of the temperature T_e.

For a negligible time delay between the onset of heating and bubble nucleation, the initial conditions for the above problem is that at time $t=0$ (moment of nucleation) the bubble radius is $R=0$ the concentration is everywhere $c=c_o$ and the temperature is everywhere $T=T_o$. The mathematical problem is extremely difficult to be solved since it contains an evolving interface in 3-D space combined with the solution of Navier–Stokes and convection–diffusion equations in moving domains. Already the corresponding 1-D moving interface problem is stiff enough due to the explosive bubble growth at the first stages and it requires special treatment for its numerical solution. Several schemes of variable transformation have been proposed in order to immobilize the moving interface. But even then, dense geometric grids are required for the discretization of the resulting equations [31,32]. So the difficulty in solving a 3-D problem of this type is obvious. Additional complexity arises for the need to resolve simultaneously the flow field generated by Marangoni convection on every instant. The Marangoni number is huge due to the large temperature gradient, rendering the numerical problem extremely stiff. Each one of the above phenomena could be resolved using state-of-the-art CFD codes (e.g. [33]) but their combination is still beyond the present capabilities of computational fluid dynamics.

2.3. Bubble motion on solid surface

From experimental observations it was found that even single bubbles can undergo lateral motion across the surface of the heater as they grow [26]. Although a naïve explanation would be to blame the action of g-jitters components parallel to the heater's surface, this cannot be a dominant effect since the motion pattern of the bubble is repeatable whereas g-jitters are not always the same. It is believed that the main reason for the lateral migration of single bubbles is thermocapillarity in a direction parallel to the heater's surface due to non-uniform curvature of the solid wall in this direction. As is shown in Section 3, the heater employed by Karapantsios and co-workers was a miniature axisymmetric thermistor. To elucidate the problem let us assume a bubble on the heater (thermistor) surface as in Fig. 3. The motion around the axis of symmetry is not considered since in that direction there is no driving force for thermocapillary migration. Due to thermocapillary convection around the bubble, which drags liquid from the hot region of the heater towards the cold bulk, the bubble is pushed towards the surface of the heater and so stays attached to it even for a zero contact angle. The possible positions of the center of the bubble are indicated by the dashed line defined as the locus of points with a distance R from the heater surface in the direction normal to the surface. Now instead of trying to solve the complete three dimensional heat transfer-fluid flow problem

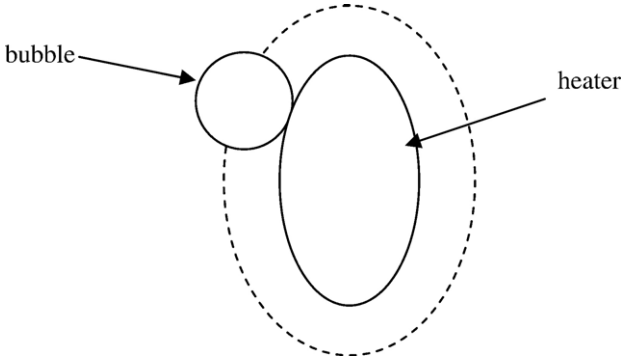

Fig. 3. A schematic of the bubble on a non-spherical heater.

one can employ the approximation of [34] (for the linear case) to find the following expression for the velocity U of the surface motion of the bubble:

$$U = \frac{f_q R}{2\mu}\left(\frac{\mathrm{d}\sigma}{\mathrm{d}T}\right)\left(\frac{\partial T_\infty}{\partial \ell}\right)_{\ell=\ell_o} \tag{18}$$

where f_q is the so-called hindrance (inverse enhancement of the drag coefficient due to proximity to a solid surface) parameter ($0<f_q<1$) depending on the distance between the bubble and the wall, T_∞ is the undisturbed temperature field (in the absence of bubble), ℓ is the length along the dashed line and ℓ_o denotes the current position of the bubble. The steady state temperature profile due to conduction in the region of a solid surface depends on the surface curvature. For convex surfaces the local temperature change is inversely proportional to the local surface curvature. This means that the derivative in Eq. (18) is non-zero and leads to a bubble motion induced by surface curvature non-uniformity with direction from the smaller to the higher curvature (convex surfaces). This motion in the present case is complicated by the existence of g-jitters and surface roughness which influences q. The gap between bubble and wall is of the order of micrometers [35] so even for a glass coated surface the roughness can influence the gap thickness and the bubble motion. Additional complication arises from the co-current growth of the bubble. As the bubble size increases, the derivative in Eq. (18) decreases radically. This may explain why the bubble motion stops as it grows larger.

2.4. Coalescence

The coalescence between multiple co-existing bubbles attached to a heated solid wall is a well known phenomenon. According to [34] there are two ways in which thermocapillarity contributes to bubble coalescence: (i) as it has been already mentioned lateral temperature gradients lead to bubble migration. But what happens in the case of an immobile bubble anchored stably on a heated wall? As already described, the bubble acts as a pump dragging liquid from the adjacent region of the hot wall and throwing it in the bulk of the liquid (jet formation). This phenomenon has been studied both theoretically [36] and experimentally [37] and there is evidence [38] that this liquid entrainment is an important mechanism for cooling (lowering the temperature) of the heater. Now as regards the coalescence of multiple bubbles, the jet created in the liquid by each bubble pulls the other bubbles towards it. (ii) Each bubble generates a radial temperature profile around it with the bubble itself being the hottest point and the temperature gradually to drop as the distance from the bubble increases. This means that any other bubble in the vicinity of the first bubble will undergo thermocapillary migration towards the first bubble. The two mechanisms can be assumed to be additive as far as the liquid entrainment described in (i) does not alter the temperature field (Marangoni number $Ma \ll 1$).

The way of action of the above two mechanisms is clearer for a pair of a large and a small bubble. The large bubble is assumed fixed in space "attracting" the mobile small bubble. The complete mathematical problem including multiple bubbles and wall interactions and non-linearity is exceedingly difficult to be solved. Several approximate solutions have been developed for the particular case $Ma \ll 1$ and Reynolds number $Re \ll 1$ exploiting the linearity of the problem. In [34], the flow and temperature fields around an immobile bubble attached to a heated wall are computed using multipole expansions and then the liquid entrainment and thermocapillary migration contributions are superimposed to give the bubble–bubble approach velocity. In a subsequent work, [35], the approach is improved adding a factor which hinders the motion of the bubble (with respect to that of the liquid) due to the existence of the solid wall. Good agreement between theoretical and experimental bubble approach velocities was found. The problem of simultaneous interaction between two equal bubbles both being free to move was solved recently employing a computational fluid dynamic code, [39]. The non-linearity has been accounted for in a heuristic way using expressions for a single bubble from [40]. In all the above cases the existence of the heated wall is represented by setting a linear velocity profile far from the wall. Setting a Dirichlet condition on the wall is not possible since there is no steady state solution for the conduction heat transfer problem in the plane geometry. In addition, inertia of the bubble was not taken into account based on the assumption of $Re \ll 1$. The mathematical problem here is much better defined than the corresponding one for the plane wall since for the present geometry the temperature field has a steady state solution so the Dirichlet boundary condition for the wall temperature can be employed. Despite the ease in formulation, the mathematical problem is very difficult to be solved for the present conditions (finite Re and Ma numbers). It is believed that in the case of non-zero Ma like the present one, convection dictates the temperature profile so only the liquid entrainment mechanism contributes to coalescence.

3. Experiment

The experimental set up has been described in detail by Divinis et al. [24,25]. Here the major components are briefly presented. The core of the equipment was an ultra-precision thermostat unit into which an exchangeable sample cell unit was inserted. For every flight, ten sample cells were taken onboard and kept under thermal control inside a second auxiliary thermostat. The cells

were specially designed to maintain their measuring chamber completely full with liquid at all times so as to prevent free float of liquid in microgravity. The pressure inside the cells was kept at ambient values by means of an elastic membrane sealing a port of the cells. This work presents only results of bubbles growing on the surface of a small, axisymmetrical, glass-coated, NTC thermistor (Thermometrics, Inc. $r_{th}=0.125$ mm, nominal) serving as a local roughly spherical heater. Bubble images from this heater were recorded by a CCD color camera with 1k × 1k pixels, 24-bit resolution RGB and acquisition rate of 25 frames per second.

Continuous heat pulses of constant power were applied to the heater through a special circuitry. The power of the pulses was constant through each run but varied among runs. Registering the voltage drop across the heater allowed the delivered power and temperature of the heater to be estimated. For all runs the bulk liquid temperature was maintained at 32 °C.

The test liquids for which results are presented here are deionized water, glycerin/water mixture 42/58% w/w and *n*-heptane (99.0%, Panreac quimica). These liquids were initially saturated by prolonged bubbling with CO_2 (99.99%, air metal). The experiments were conducted during the 35th and 38th ESA's Parabolic Flight Campaigns (PFC). Each run was conducted during a separate parabola with the acceleration of gravity fluctuating within $\pm 2.6\times 10^{-2}$ g. The low gravity period was slightly different among parabolas but on the average lasted approx. 20 s.

4. Results–discussion

The main effort so far in this lab has been focused on the problem of single dissolved-gas bubbles growing over heated surfaces. The problem is rather prototype and has not been studied in literature perhaps due to the serious disturbances created by gravity. To get the right picture, it is important to review first the main features of the experimental growth curves as observed under microgravity conditions [24–26]. In all examined fluids, bubbles grow fast at the beginning and gradually slow down at later stages. The bubble growth rates measured in *n*-heptane are much higher than those measured in water and glycerin/water solutions. This is so despite the fact that the heating powers (and heater temperatures) employed in *n*-heptane are the lowest of all. Thus, the physical properties of the test liquid appear to dictate the rate of growth over and above the input power (heater temperature). Another significant observation is that for the same liquid, increasing the temperature of the heater produces progressively larger bubbles. This does not continue infinitely but stops at a certain temperature (different for each liquid) beyond which any further increase has no significant effect on the size of the bubble.

Our first approach to cope theoretically with the problem was based on the naïve assumption of a uniform temperature along the surface of the bubble, equal to that of the heating surface T_e. The geometrical complications were ignored and the one-dimensional bubble growth problem was considered. The existence of the heating surface was replaced in the 1-D approximation (spherical system of coordinates) by a heat source inside the bubble. This 1-D problem was similar to the well-known problem of gas bubble growth inside infinite liquids of constant supersaturation controlled by heat and mass transfer [14]. Based on the experimental data for the thermistor temperature ($T_e \cong$ constant, see below), an analysis was performed first for the case of constant (in time) and uniform (in space) bubble temperature. Using standard techniques it was found that the mathematical problem exhibits a self-similarity solution implying a square root dependence of the growing bubble radius on time. The key feature of this (self-similar) solution is that the concentration and temperature profiles in the liquid have a time independent shape provided that the spatial dimension is scaled with the increasing bubble radius. The evolution of the bubble radius is given as:

$$R = 2\beta\sqrt{\alpha t} \tag{19}$$

where $\alpha = k/(\rho_1 c_p)$ is the thermal diffusivity of the liquid. The temperature and concentration profiles with respect to the spherical coordinate r, are given as:

$$\frac{T - T_o}{T_e - T_o} = \frac{I(s,\beta)}{I(\beta,\beta)} \tag{20}$$

$$\frac{c - c_{eq}(T_o)}{c_{eq}(T_e) - c_{eq}(T_o)} = \frac{I(\lambda s, \lambda\beta)}{I(\lambda\beta, \lambda\beta)} \tag{21}$$

where $\lambda = \sqrt{\frac{\alpha}{D}}$, and $s = \frac{r}{2\sqrt{\alpha t}}$ is the self-similarity variable. The function I is given from the integral $I(x,\beta) = \int_x^\infty \frac{1}{y^2} e^{-y^2 - 2\beta^3/y} dy$. The parameter β is found from the solution of the following transcendental equation:

$$\varphi(\beta\lambda) = \varphi(\beta\lambda, \beta\lambda) 2(\beta\lambda)^3 e^{3(\beta\lambda)^2} = F_m \tag{22}$$

where

$$F_m = \frac{(c_{eq}(T_e) - c_{eq}(T_o))R_g T_e}{P_b - P_L(T_e)} \tag{23}$$

The parameter F_m is the main dimensionless parameter of the bubble growth problem and since it is similar to the one

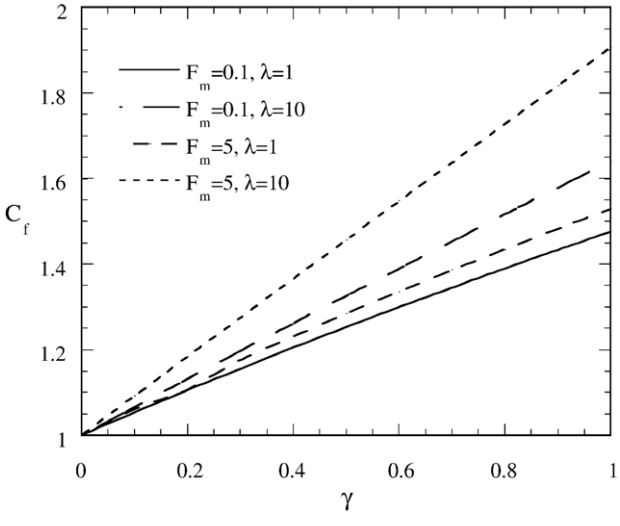

Fig. 4. Dependence of the correction factor C_f on the slope γ of the diffusivity–temperature linear dependence for several pairs of the parameter λ and the Foaming number F_m.

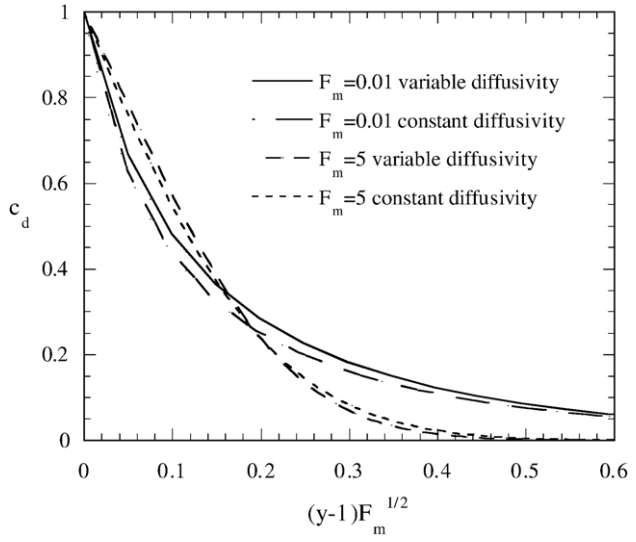

Fig. 5. Dimensionless concentration profile in the liquid for variable (γ=0.5) and constant (γ=0) diffusivity and for two values of the Foaming number F_m.

called Foaming number in the polymer foaming literature (e.g. [41]), this terminology is adopted here. The Foaming number is actually the ratio of the convection (induced by the bubble surface expansion) to the diffusion contribution to the bubble growth rate. It is worth to note that the diffusivity does not appear explicitly in the Foaming number since convection is also proportional to diffusivity (as diffusion) so it is eliminated between the numerator and the denominator and only net driving forces eventually show up in the ratio. The energy input rate, W, to the bubble needed to ensure bubble growth under a constant temperature, varies also with the square root of time:

$$W = 16\pi\beta^3\left(k(T_e - T_o)\frac{1}{\varphi(\beta)}\right)\sqrt{\alpha t} \tag{24}$$

The above solution is based on the assumption of constant transport properties k and D. Yet, the temperature profile established around the bubble implies that the local temperature can vary in a range of several decades of degrees Celsius leading to a variation of the diffusion coefficient even up to 300% [25]. This means that the variation of the transport properties of the liquid must be taken into account in the bubble growth problem. A variation of the diffusion coefficient with respect to the gas concentration has been considered previously in [42] and [43]. The above authors showed that a self-similar solution still exists but the constant $\beta\lambda$ had to be found from the numerical solution of a non-linear boundary value problem. Asymptotic solutions were given for the cases of small and large F_m. The situation here is more complicated since there are two fields dictated by diffusion–convection type of equation and they are fully coupled through the fluid velocity dependence on mass transfer and diffusivity dependence on the temperature. It was shown [44] that even in this case a self-similar solution to the problem can still be derived. But now the growth constant has to be found from the solution of a complicated boundary value problem. Alternatively, the following approximated explicit solution derived in [44] can be used:

$$R = \sqrt{2PD(T_o)t} \tag{25}$$

where

$$P = D_m\,\bar{P} \tag{26}$$

$$\bar{P} = 2(0.7063 + 0.4545\sqrt{F_m} + 0.1591F_m)^2F_m \quad \text{for } F_m<0.89 \tag{27a}$$

$$\bar{P} = 2(F_m + 0.3232)^2 \quad \text{for } 0.89<F_m<5.7 \tag{27b}$$

$$\bar{P} = 2(F_m\sqrt{3/\pi} + 4/9)^2 \quad \text{for } F_m>5.7 \tag{27c}$$

$$\frac{T - T_o}{T_e - T_o} = \frac{\int_y^\infty x^{-2}e^{-(x^{-1}+x^2/2)\frac{\bar{P}}{\lambda^2 k_m}}dx}{\int_1^\infty x^{-2}e^{-(x^{-1}+x^2/2)\frac{\bar{P}}{\lambda^2 k_m}}dx} \tag{28}$$

$$k_m = \frac{k(T_e) + (T_o)}{2k(T_o)} \tag{29}$$

$$D_m = \left(\int_1^\infty \frac{D(T_o)}{x^2D(T)}e^{-\frac{D(T_e)}{D(T_o)}\bar{P}(x^{-1}+x^2/2)}dx\right)^{-1} \times \int_1^\infty \frac{1}{x^2}e^{-\frac{D(T_e)}{D(T_o)}\bar{P}(x^{-1}+x^2/2)}dx \tag{30}$$

The notation $D(T)$ and $k(T)$ denotes the dependence of the gas-in-liquid diffusivity and liquid conductivity on temperature. The growth factor P is related to β in Eq. (19) through: $P=2\beta^2\lambda$.

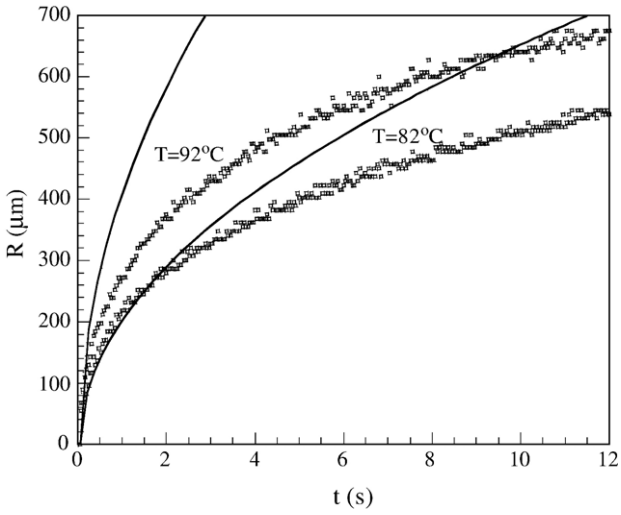

Fig. 6. Experimental and approximated (constant bubble temperature) bubble radius evolution curves for the system CO_2–water and two heater temperatures.

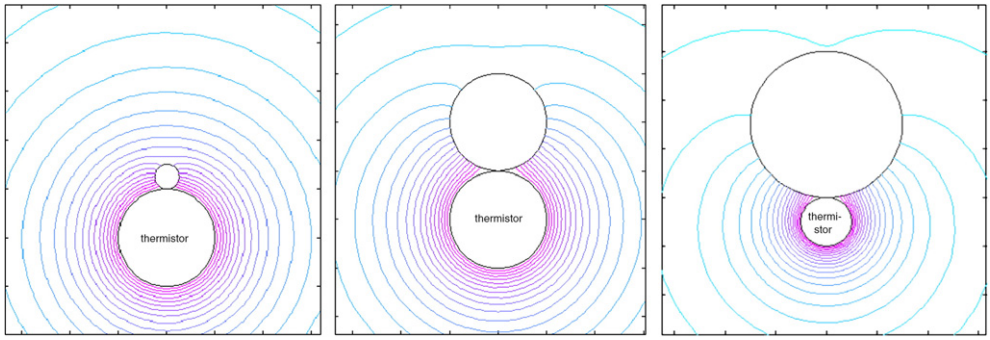

Fig. 7. Isotherms (with spacing $0.05(T_e - T_o)$) in the liquid around the bubble–heater system for three values of the bubble-to-heater radius ratio (q=0.25, 1, 3, respectively).

In order to get some quantitative feeling of the effect of the temperature dependent diffusivity on bubble growth rate, a linear diffusivity–temperature relation is assumed:

$$D(T) = D(T_o)\left(1 + \gamma \frac{T - T_o}{T_e - T_o}\right) \tag{31}$$

where γ is a coefficient varying between 0 and 1.

The ratio C_f of the growth factor P for the diffusivity given by Eq. (31) to the growth factor for constant diffusivity ($D(T)=D(T_o)$) is shown in Fig. 4 for two values of the Foaming number and two values of the parameter λ. It is interesting that the $C_f(\gamma)$ curves can be approximated by straight lines with zero intercept up to values of γ equal to unity. In general, the increase of the F_m number, increases the influence of the diffusivity–temperature dependence on bubble growth. The (self-similar) profiles of the dimensionless gas concentration ($c_d=(c-c_o)/(c_{eq}(T_e)-c_o)$) in the liquid for constant and temperature dependent diffusivity (γ=0.5) and for two values of F_m are shown in Fig. 5. It is obvious that the effect of temperature dependent diffusivity is to make the concentration profile steeper.

An attempt to compare the theoretical growth curves based on a constant bubble temperature (that of the heater) approximation to the corresponding experimental curves revealed that whereas the theoretical $t^{1/2}$ behavior is followed at the early stages of bubble growth, at later stages the actual growth rate is smaller than the theoretical one. A typical comparison between the experimental and the theoretical growth curves for CO_2 bubbles in water and two values of heater temperatures is shown in Fig. 6. It is clear that only data obtained at microgravity conditions could address this issue because then bubbles are allowed to grow for several seconds and become sufficiently large without distortion from sphericity, departure from the heater or natural convection currents in the liquid around them. The stronger proof, however, for the failure of the constant bubble temperature approximation is the fact that the heating rate required to keep the bubble growing at constant temperature soon exceeds the power given by the heater [24]. The bubble actually has to grow in the temperature field developed around the heater and based on the local liquid–gas temperature equilibrium, a 3-D temperature profile is

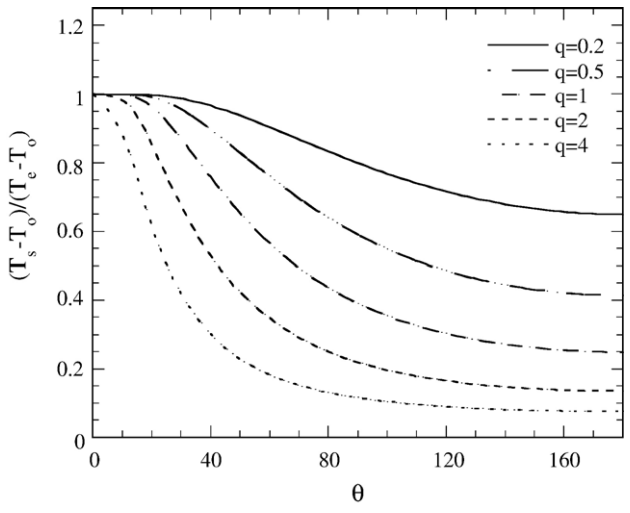

Fig. 8. Dimensionless temperature on the surface of the bubble versus the angle θ for several values of bubble-to-heater radius ratio q. θ=0 represents the contact point of the bubble to the heater.

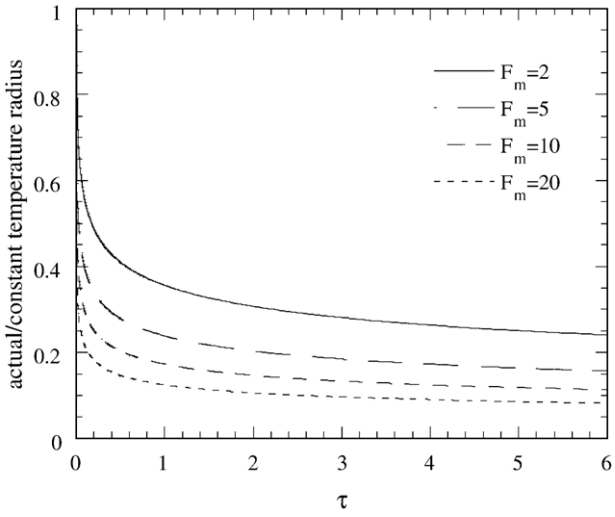

Fig. 9. Evolution of the ratio of the radius of a bubble growing non-isothermally (with just a single point contact with the isothermal heater, $T_e \cong$ constant), to the radius of a bubble growing altogether isothermally (at the temperature of the heater $T=T_e \cong$ constant), for several values of the foaming number F_m (dimensionless time $\tau = Dt/R_h^2$).

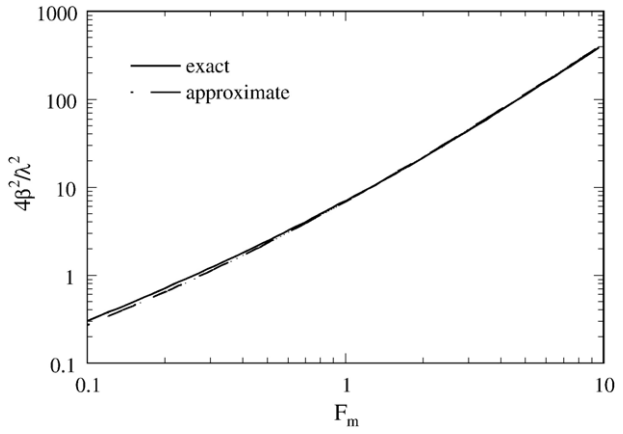

Fig. 10. Comparison between exact (Eq. (22)) and approximate (based on Eq. (38)) values of the bubble growth constant.

developed in the bubble. As the bubble grows it is exposed to colder liquid so the growth rate is reduced compared to the one corresponding to the constant bubble temperature. This is shown schematically in Fig. 7 where one can see the temperature contour plots at three stages of the bubble evolution. Initially the bubble is very small, its temperature is very close to that of the heater and the initial $t^{1/2}$ behavior of the experimental curves can be explained. So the existence of the heated surface creates an intra-bubble temperature distribution and destroys the self-similarity of the mathematical problem. The Marangoni motion set up by the temperature variation on the surface of the bubble acts to bring the bubble back to the heater temperature (i.e. to weaken the effect of the 3-D geometry on bubble growth).

In order to quantitatively assess the influence of the geometry and to confirm the reduced bubble growth rate observed experimentally, an approximate solution to the bubble growth problem on a spherical heater was attempted in [45]. The Marangoni effect was ignored in order to find the maximum

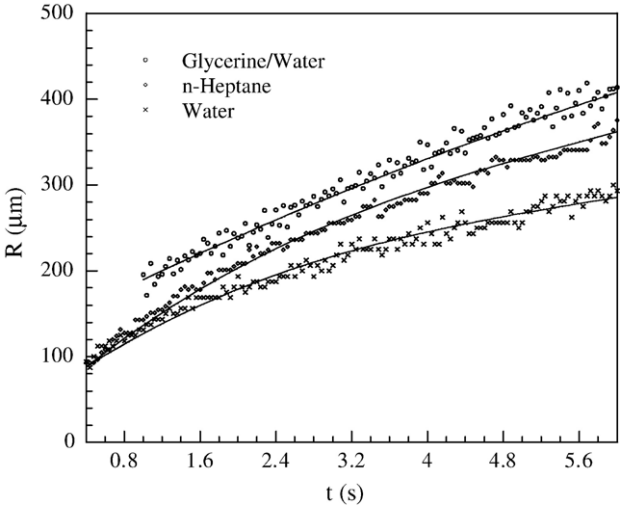

Fig. 11. Experimental bubble radius evolution curves (symbols) and the corresponding fitted curves employed by the inverse problem procedure for CO_2 dissolved in three different liquids.

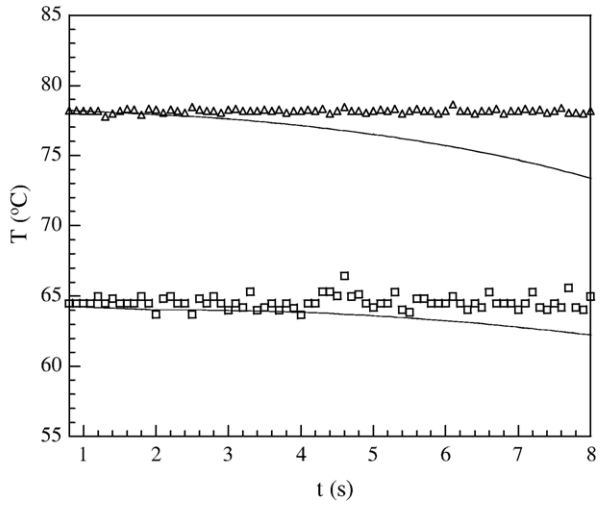

Fig. 12. Measured heater temperature (symbols) and estimated by the inverse problem approach average bubble temperature for the system CO_2–water for two different heating runs (two different heater temperatures).

possible influence of the geometry on the bubble growth rate. In addition, it was assumed that the heat transfer dynamics is faster than mass transfer dynamics so a pseudo-steady state temperature distribution in the liquid could be used. This distribution was found by solving the conduction equation in bispherical coordinates using the separation of variables technique. The temperature distribution on the surface of the bubble is used in order to find the local equilibrium concentration of the dissolved gas and the average gas density in the bubble. Finally, assuming a large Foaming number and invoking the results shown in [23] the diffusion–convection equation was solved locally on a thin boundary layer. The resulting set of equations for the evolution of the bubble radius is:

$$\frac{dR}{dt} = DR^2 F_m \frac{1}{\bar{\rho}_{gave}\sqrt{\pi}} \frac{1}{\sqrt{g}} \left(1 + \int_{g'=0}^{g} \frac{\partial \Phi(R)}{\partial g'} \frac{\sqrt{g}}{\sqrt{g-g'}} dg' \right) \tag{32}$$

$$\frac{dg}{dt} = DR^4 \tag{33}$$

where

$$\Phi(R) = \int_0^{\pi} \left(\frac{c_{eq}(T_s) - c_o}{c_{eq}(T_e) - c_o} \right) \frac{(1-\cos\theta)\sin\theta}{2} d\theta \tag{34}$$

$$\bar{\rho}_{gave} = \frac{1 - x_{vave}}{(1 - P_L(T_e)/P_b)} \frac{T_e}{T_{gave}} \tag{35}$$

$$T_{gave} = \frac{1}{2} \int_0^{\pi} T_s(\theta) \sin\theta d\theta \tag{36}$$

$$x_{vave} = \frac{1}{2P_b} \int_0^{\pi} P_L(T_s) \sin\theta d\theta \tag{37}$$

$T_s = T_s(\theta)$ is the temperature profile on the bubble surface and can be found from the closed form series solution for the

temperature field in the bispherical system of coordinates. This temperature profile is shown in Fig. 8 for several values of the bubble-to-thermistor radius ratio q ($q=R/R_h$ where R_h is the radius of the spherical thermistor) and several angular positions, θ, around the bubble. It is evident in the Figure that the local angular temperature on the bubble decreases as its size increases. For large bubbles only a small portion of the bubble close to the heater can "feel" the temperature of the heater. The ratio of the bubble radius growing on a heater of temperature T_e to the bubble radius growing at constant temperature T_e is shown in Fig. 9. This Figure is in accordance with the experimental finding that the $t^{1/2}$ rule is obeyed initially but then the growth rate is reduced. It must be stressed though that the reduction in practice is smaller than the one displayed in Fig. 9 due to the counterbalancing effect of the Marangoni phenomenon which was not accounted for in the above analysis. Furthermore, it must be noted that both the experimental and theoretical $R(t)$ curves can be fitted by power law curves with exponents smaller than 0.5 which is in accordance with the bubble growth behavior observed during boiling experiments under microgravity conditions [21].

The above approximate solutions for the bubble growth problem are capable of giving only the two (upper and lower) bounds for the actual situation. The direct solution of the complete problem (including Marangoni convection) is not feasible at present as it has been already referred and consequently the inverse problem of estimation of unknown parameters from experimental results is out of the question.

In order to exploit the microgravity experimental results of bubble growth data and heater temperatures, the actual problem is approximated by the one dimensional problem of a bubble growing at a uniform but time dependent temperature. This one-dimensional problem is based on a completely different approach than the one presented above based on the uniform temperature assumption. Above, the computation could be performed only after assuming that the bubble temperature is spatially uniform. Here, uniformity simply refers to a spatially average value of the bubble temperature predicted from a fitting procedure of the data although it is fully understood that the bubble surface has actually a non-uniform temperature. The predicted temperature must be a good approximation of the surface average of the actual bubble temperature. So, by solving

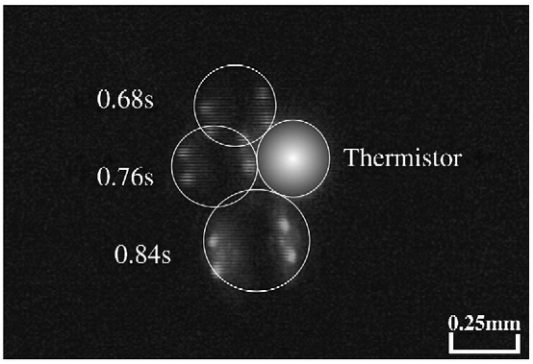

Fig. 13. Instants during bubble displacement across the surface of the spherical heater (thermistor), $T_{thermistor}=45$ °C.

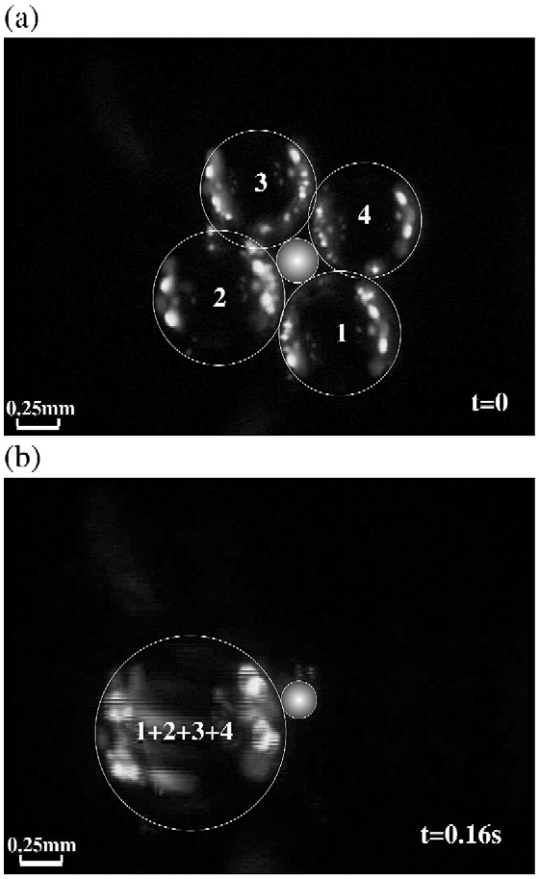

Fig. 14. Coalescence of four (4) bubbles attached to the spherical heater at (a) $t=0$ s and (b) $t=0.16$ s, $T_{thermistor}=80$ °C.

the inverse problem based on experimental bubble growth curves the evolution of the spatially average bubble temperature can be inferred. But still the simplified problem consists of partial differential equations with moving boundaries making the inversion procedure very elaborate. For this reason a simplified solution to the direct problem has been developed in [25]. A pseudo-steady state temperature profile was assumed and explicit asymptotic solutions were derived in the limits of small and large Foaming number for the general case of time dependent bubble temperature. The two asymptotes were combined using a generalized interpolation rule to get an equation valid for all values of F_m:

$$\frac{dR}{dt}=\frac{1}{R}\left(\left[F_m D\left(\frac{T_o+T_b}{2}\right)\right]^{-0.8}+\left[\frac{6}{\pi}F_m^2 D(T_b)\right]^{-0.8}\right)^{-1.25} \tag{38}$$

where $T_b=T_b(t)$ is the unknown spatially average temperature of the bubble surface and $D(T)$ denotes the temperature dependence on diffusivity. In the case of a constant bubble temperature and diffusivity independent from temperature ($T_b=T_e$) the mathematical problem exhibits the self-similarity solution already described. In this case the approximate Eq. (38) also predicts the $t^{1/2}$ radius dependence with a growth factor β/λ very close to the exact one as shown in Fig. 10. Using this

approximate solution, the inverse problem becomes trivial; the temperature evolution $T_b(t)$ can be found from the solution of the algebraic equation:

$$\left(\left[2F_m D\left(\frac{T_o+T_b}{2}\right)\right]^{-0.8}+\left[\frac{12}{\pi}F_m^2 D(T_b)\right]^{-0.8}\right)^{-1.25}=\left(\frac{dR^2}{dt}\right)_{exp} \quad (39)$$

The time derivatives $\left(\frac{dR^2}{dt}\right)_{exp}$ are computed by first fitting low order polynomials to the R^2 experimental curves and then differentiating them analytically. To get an idea of the fitting quality, typical experimental $R(t)$ curves for several liquids and the corresponding fitted curves are shown in Fig. 11. The result of the inverse problem is the estimation of the average bubble temperature and a typical case for CO_2 bubbles growing in water is shown in Fig. 12. Again, it was the microgravity conditions that allowed comparisons for so many seconds. It is clear that the bubble temperature soon gets smaller than that of the heater with the difference increasing with the bubble size, as it has been already analyzed. In reality, the discrepancy should be actually smaller than that shown in Fig. 12 which represents the theoretically determined lower bound. This is so because the contribution of the Marangoni effect which acts to rise the bubble temperature was not included in the analysis.

Regarding the bubble lateral motion across the heater and coalescence phenomena typical experimental results are shown in Figs. 13 and 14. Fig. 13 presents a series of instants where a bubble moves around a miniature heater (a glass-coated thermistor) in the system CO_2/*n*-heptane. Nucleation occurs at $t=0$ s. The bubble grows initially at its nucleation site for 0.68 s, followed by a short living travel to another position where it stops (0.84 s) and continues to grow without any further movement. As can be seen, the bubble starts to move when it gets roughly as large as the heater. This manifests the significance of the relative curvatures of the heater and the bubble which combined with the low values of interfacial tension and contact angle in the system *n*-heptane/CO_2/glass, can destabilize the three phase contact line and trigger the motion. Yet, these factors alone could only yield an instantaneous new contact line without any significant lateral motion. Therefore, it seems reasonable to assume that the motion, once triggered by the above factors, is further sustained by thermocapillarity which drags the bubble towards hotter regions around the heater.

When multiple bubbles grow simultaneously on a miniature heater, clustering and coalescence are witnessed. Fig. 14(a) shows four bubbles in contact with the heater and each other. It only takes a small disturbance (g-jitter) to rupture this cluster and make all four bubbles coalesce into one. The collapse occurs so fast that, with our recording capacity, we capture only blurred images of the intermediate events (not shown). After 0.16 s, the newly formed large bubble is at rest and continues to grow until the heat pulse is over.

In order to include the bubble lateral motion and coalescence phenomena in a global analysis of the non-isothermal degassing problem an extension of earlier formulations along with a series of simplifications must be performed. As explained in a previous section, there is already some experience accumulated by other works on the subject but it remains to be quantitatively adjusted and extended for the particular problem.

5. Conclusions

In this work the current level of knowledge and understanding of the phenomena occurring during the non-isothermal degassing of liquids is reviewed. Data obtained over several seconds under microgravity conditions allowed for the first time to conduct safe comparisons between experiments and theoretical predictions. The excessive complexity arising from the interrelationship among the occurring phenomena, forced us to separate them and examine them one by one. Whereas the phenomena of bubble motion and bubble coalescence on a heated wall can be analyzed using existing techniques and approximations, the gas bubble growth on a heated wall requires further fundamental analysis. The complete mathematical problem is formulated and given the inability to solve it numerically with the present resources, a series of approximations is attempted and the results are presented. Whereas up to now the results are encouraging showing fair agreement with experimental observations and contributing to the understanding of the whole complex process, further analysis is needed mainly related to the quantitative assessment and computation of the Marangoni effect around the bubble.

References

[1] Payvar P. Mass transfer controlled bubble growth during rapid decompression of a fluid. Int J Heat Mass Transfer 1987;30:699–706.
[2] Barker GS, Jefferson B, Judd SJ. The control of bubble size in carbonated beverages. Chem Eng Sci 2002;57:565–73.
[3] Malley JP, Edzwald JK. Concepts for dissolved-air flotation treatment of drinking waters. Water SRT Aqua 1991;40:7–17.
[4] Heide K, Hartmann E, Stelzner Th, Müller R. Degassing of a cordierite glass melt during nucleation and crystallization. Thermochim Acta 1996;280–281: 243–50.
[5] Yamasaki M, Iwamoto K, Tamagawa H, Kawamura Y, Lee JK, Kim HJ, Bae JC. Vacuum degassing behavior of Zr-, Ni- and Cu-based metallic glass powders. Mater Sci Eng A 2007;449:907–10.
[6] Nyborg L, Magalhuaes S. Hot degassing of high alloy metal powders. Met Powder Rep 1996;51:38–53.
[7] Harding GL, Window B. Degassing of hydrogenated metal–carbon selective surfaces for evacuated collectors. Sol Energy Mater 1982;7:101–11.
[8] McCabe WL, Smith JC. Unit Operations of Chemical Engineering. 2nd edition. McGraw-Hill; 1967.
[9] Perry RH, Chilton CH. Chemical Engineer's Handbook. McGraw-Hill Kogakusha international student edition 5th edition. 1973.
[10] Szekely J, Fang SD. Non-equilibrium effects in the growth of spherical gas bubbles due to solute diffusion—II: The combined effects of viscosity, liquid inertia, surface tension and surface kinetics. Chem Eng Sci 1973;28:2127–40.
[11] Kern DQ. Process Heat Transfer. NY: McGraw-Hill; 1950.
[12] Plesset MS, Zwick SA. The growth of vapor bubbles in superheated liquids. J Appl Phys 1954;25:493–500.
[13] Forster HK, Zuber N. Growth of a vapor bubble in a superheated liquid. J Appl Phys 1954;25(4):474–8.
[14] Scriven LE. On the dynamics of phase growth. Chem Eng Sci 1959;10: 1–13.
[15] Glas JP, Westwater JW. Measurements of the growth of electrolytic bubbles. Int J Heat Mass Transfer 1964;7:1427–43.

[16] Bisperink CGJ, Prins A. Bubble growth in carbonated liquids. Colloids Surf A Physicochem Eng Asp 1994;85:237–53.
[17] Jones F, Evans GM, Galvin KP. The cycle of bubble production from a gas cavity in a supersaturated solution. Adv Colloid Interface Sci 1999;80: 51–84.
[18] Jones F, Evans GM, Galvin KP. Bubble nucleation from gas cavities — a review. Adv Colloid Interface Sci 1999;80:27–50.
[19] Strenge PH, Orell A, Westwater JW. Microscopic study of bubble growth during nucleate boiling. AIChE J 1961;7:578–83.
[20] Saddy M, Jameson GJ. Experiments on the dynamics of phase growth. Chem Eng Sci 1971;26:675–84.
[21] Picker G, Straub J. "Interfacial mass transfer studies on vapor bubbles in microgravity", *In Proc. United Engineering Foundation conference* (Sept. 1999), Kahuku, Oahu, Hawaii.Ed. Dhir, 72–79 (2000).
[22] Westerheide DE, Westwater JW. Isothermal growth of hydrogen bubbles during electrolysis. AIChE J 1961;7:357–62.
[23] Buehl WM, Westwater JW. Bubble growth by dissolution: influence of contact angle. AIChE J 1966;12:571–6.
[24] Divinis N, Karapantsios TD, Kostoglou M, Panoutsos CS, Bontozoglou V, Michels AC, et al. Bubbles growing in supersaturated solutions at reduced gravity. AIChE J 2004;50:2369–82.
[25] Divinis N, Karapantsios TD, de Briyin R, Kostoglou M, Bontozoglou V, Legros J. Bubble dynamics during degassing of dissolved gas saturated solutions at microgravity conditions. AIChE J 2006;52:3029–40.
[26] Divinis N, Karapantsios TD, de Briyin R, Kostoglou M, Bontozoglou V, Legros J. "Lateral motion and interaction of gas bubbles growing over spherical and plate heaters". Microgravity Science and Technology 2006;18:204–9.
[27] Merte Jr H, Lee HS. Quasi-homogeneous nucleation in microgravity at low heat flux: experiments and theory. J Heat Transfer 1997;119:305–12.
[28] Lee HS, Merte Jr H, Picker G, Straub J. Quasi-homogeneous boiling nucleation on a small spherical heater in microgravity. Int J Heat Mass Transfer 2003;46:5087–97.
[29] Fogg PGT, Gerrard W. Solubility of Gases in Liquids: A Critical Evaluation of Gas Liquid Systems in Theory and Practice. New York: Wiley Interscience; 1991.
[30] Cable M, Frade JR. The influence of surface tension on the diffusion-controlled growth or dissolution of spherical bubbles. Proc R Soc Lond A 1988;420:247–65.
[31] Arefmanesh A, Advani SG, Michaelides EE. An accurate numerical solution for mass diffusion induced bubble growth in viscous liquids containing limited dissolved gas. Int J Heat Mass Transfer 1992;35:1711–22.
[32] Prousevitch AA, Sahagian DC, Anderson AJ. Dynamics of diffusive bubble growth in magmas. J Geophys Res 1983;98:22283–307.
[33] Wang H, Peng XF, Cristopher DM, Lin WK, Pan C. Investigation of bubble-top jet flow during sub-cooled boiling on wires. Int J Heat Fluid Flow 2005;26:485–94.
[34] Guelcher SA, Solomentsev YE, Sides PJ, Anderson JL. Thermocapillary phenomena and bubble coalescence during electrolytic gas evolution. J Electrochem Soc 1998;145:1848–56.
[35] Kasumi H, Solomentsev Y, Guelcher S, Anderson J, Sides P. Thermocapillary flow and aggregation of bubbles on solid wall. J Colloid Interface Sci 2000;232:111–20.
[36] Arlabosse P, Lock N, Medale M, Jaegger M. Numerical investigation of thermocapillary flow around a bubble. Phys Fluids 1999;11:18–29.
[37] Kao YS, Kenning DBR. Thermocapillary flow near a hemispherical bubble on a heated wall. J Fluid Mech 1972;53:715–32.
[38] Lu JF, Peng XF. Bubble separation and collision on thin wires during subcooled boiling. Int J Heat Mass Transfer 2005;48:4726–37.
[39] Kasumi H, Sides PJ, Anderson JL. Interactions between two bubbles on a hot or cold wall. J Colloid Interface Sci 2004;276:239–47.
[40] Subramanian RS, Balasubramanian R. The Motion of Bubbles and Drops in Reduced Gravity. New York: Cambridge University Press; 2001.
[41] Yoo HJ, Han CD. Oscillatory behavior of a gas bubble growing (or collapsing) in viscoelastic liquids. AIChE J 1982;28:1002–9.
[42] Lastochkin D, Favelukis M. Bubble growth in variable diffusion coefficient liquid. Chem Eng J 1998;69:21–5.
[43] Cable M, Frade JR. Diffusion-controlled mass transfer to or from spheres with concentration-dependent diffusivity. Chem Eng Sci 1987;42:2525–30.
[44] Divinis N, Kostoglou M, Karapantsios TD, Bontozoglou V. Self-similar growth of a gas bubble induced by localized heating: the effect of temperature-dependent transport properties. Chem Eng Sci 2005;60:1673–83.
[45] Kostoglou M, Karapantsios TD. Approximate solution for a nonisothermal gas bubble growth over a spherical heating element. Ind Eng Chem Res 2005;44:8127–35.